Received: 30 November 2022 | Revised: 31 January 2023 | Accepted: 5 February 2023

DOI: 10.1002/zamm.202200567

ORIGINAL PAPER

Dynamics of forced escape from asymmetric truncated parabolic well

Attila Genda[1] | **Alexander Fidlin**[1] | **Oleg Gendelman**[2]

[1]Institute of Engineering Mechanics, Karlsruhe Institute of Technology, Karlsruhe, Germany

[2]Mechanical Engineering, Technion - Israel Institute of Technology, Haifa, Israel

Correspondence
Attila Genda, Institute of Engineering Mechanics, Karlsruhe Institute of Technology, Karlsruhe, Germany.
Email: attila.genda@kit.edu

Present address
Attila Genda , Building 10.23, 1st floor, Room 101, Kaiserstr. 10 76131, Karlsruhe, Germany

Funding information
Deutsche Forschungsgemeinschaft, Grant/Award Number: 508244284

This study presents an analytic method for the estimation of safe basins in the plane of the initial conditions of the escape of a classical particle from an asymmetrically truncated quadratic potential well. For this purpose, an analytic method to estimate the global optimum of the sum of two harmonic functions is proposed. This approach is based on the mapping of the arguments of the two harmonic terms to the surface of the unit torus, where a surrogate optimization problem obtained by the Taylor expansion of the original objective function is solved. Applying the proposed method to the aforementioned escape problem helps predict safe basins for any value of the excitation frequency provided that the exciting force is not too strong, generating essentially non-linear effects on potential boundaries. Specifically, interesting effects with regard to the shape of safe basins occur when the natural frequency of the potential well and frequency of excitation represent the ratio of two small integers.

1 | INTRODUCTION

Escape from a potential well is a well-known topic in the theory of non-linear dynamic systems [1–5]. The escape-related phenomena range from chemical reactions [6, 7] through the physics of Josephson junctions [8] and MEMS devices [9–14] to celestial mechanics and gravitational collapse. Escape plays a role in energy harvesting [15] and is related to the transient resonance dynamics of oscillatory systems [16, 17] and specific phenomena, for example, the capsizing of ships [4, 18]. Several studies have been conducted in the last 80 years in the field of escape; however, there are many unresolved issues that require investigation [19].

Various aspects of escape can be investigated. The problem of the sharp minimum of the critical excitation amplitude depicted by excitation frequency in the vicinity of the main resonance using unlimited potential with the main aspect based on homogeneous initial conditions (ICs) is addressed in [20]. The effect of two strongly coupled particles on the escape behavior in a truncated quadratic potential focusing on the vicinity of the main resonance is investigated in ref. [21]. The determination of the hyper-volume (in 2D: area) of safe basins (SBs), that is, a set of non-escaping ICs under certain excitation and the investigation of various integrity measures, introduced to describe the technically relevant size of the non-escaping set, received considerable attention [2, 22–24]. The investigated potential wells were non-quadratic; therefore, accurate analytic results cannot be provided to describe SB boundaries. Approximations using Melnikov's method

[2] or adiabatic invariants and action-angle variables [25] provide analytic formulas in the vicinity of the main resonance for small excitation values; however, estimates become inaccurate if they are far from $1:1$ resonance.

In this study, the SBs of the escape of a single particle from an asymmetrically truncated quadratic potential well under harmonic excitation are investigated. The selected potential is probably the simplest one, as the motion of the particle inside the well can be given in an analytically closed form, not only for small excitation around the main resonance but also in general. In ref.[26], the symmetrical case with the incommensurable excitation frequency/natural frequency ratio was considered, leaving the case of a commensurable frequency ratio as an open question. However, if the ratio of the excitation's frequency and the natural frequency of the potential well is a small rational number, that is, $N:M$, interesting effects occur, leading to the enlargement of the SB compared to the case when the frequency ratio is slightly disturbed. In certain cases, there is a substantial difference in the existence of SBs: a SB exists if the ratio of the excitation frequency to the natural frequency is $1:M$; however, owing to the effect of the slightest disturbance on this ratio, the SB disappears. This result indicates that SBs may possess structurally unstable and stable parts. Numerical simulations do not always reveal this fact; owing to additional disturbance in the frequency ratio, the escape time in the structurally unstable part of the SB might extend; thus, the simulation might stop before the particle escapes. This concern with regard to the robustness of the SB is even worse in the aforementioned case of $1:M$ excitation; then, the whole area of the SB might be structurally unstable.

For the quantitative prediction of the aforementioned basins, Section 2 introduces an accurate method for the estimation of the global optima of the sum of two harmonics. In Section 3, the estimation is applied to the specific case of escape from an asymmetrically truncated quadratic potential well with harmonic excitation, where the two harmonic terms of the function to be estimated result from the homogeneous and particular solutions of the underlying differential equation, describing the motion of the particle inside the potential well. Section 4 compares the analytical results to that of numeric simulations, thereby demonstrating the accuracy of the proposed method by comparing the global integrity measures derived either way. Section 5 provides suggestions on further studies and concludes the current study.

2 | GLOBAL OPTIMUM OF THE SUM OF TWO HARMONICS

Before starting to investigate the problem with regard to the SBs of escape, let us investigate a mathematical optimization problem. The results will be necessary in this study, as the motion of a harmonic oscillator excited with a sinusoidal force is the sum of two harmonics with different frequencies. We are looking for the

$$\sup_{\tilde{t}} f(\tilde{t}) = \sup_{\tilde{t}} A\cos(\tilde{\Omega}_A\tilde{t}+\tilde{\alpha}_A) + B\cos(\tilde{\Omega}_B\tilde{t}+\tilde{\alpha}_B) \tag{1}$$

for $A, B, \tilde{\Omega}_A, \tilde{\Omega}_B \in \mathbb{R}^+$ and $\tilde{\alpha}_A, \tilde{\alpha}_B \in [0, 2\pi)$ with "sup" standing for supremum. With the coordinate transformation

$$t := \tilde{\Omega}_A\tilde{t} + \tilde{\alpha}_A \tag{2}$$

and

$$\Omega_B := \frac{\tilde{\Omega}_B}{\tilde{\Omega}_A}, \tag{3}$$

$$\alpha_B := -\frac{\tilde{\Omega}_B\tilde{\alpha}_A}{\tilde{\Omega}_A} + \tilde{\alpha}_B, \tag{4}$$

the problem can be rewritten as

$$f_{\sup} := \sup_t f(t) = \sup_t(A\cos t + B\cos(\Omega_B t + \alpha_B)). \tag{5}$$

If the frequencies $\tilde{\Omega}_A$ and $\tilde{\Omega}_B$ are commensurable, that is, Ω_B is rational, function $f(t)$ is periodic, and being a bounded function, its supremum is taken at some value of t, hence, it has a global maximum, indeed. In case Ω_B is irrational, function $f(t)$ is only almost periodic and does not have a well defined global maximum. Instead, it passes arbitrarily close to its supremum given by $A + B$ for some values of t.

Theorem 1. *In case of $\Omega_B \in \mathbb{R}\backslash\mathbb{Q}$ (i.e., an irrational number), the supremum of Equation (5) is*

$$f_{sup,Irr} := A + B. \tag{6}$$

In case of $\Omega_B \in \mathbb{Q}$, we have that $\Omega_B = N/M$ with some $N, M \in \mathbb{N}$. Then, f_{max} can be estimated by

$$f_{max,Rat} := A\left(1 - 2\pi^2\left(\frac{B\Omega_B}{A + B\Omega_B^2}\right)^2 |y_0|^2\right) + B\left(1 - 2\pi^2\left(\frac{A}{A + B\Omega_B^2}\right)^2 |y_0|^2\right), \tag{7}$$

with

$$\Delta E = \frac{\gcd(M,N)}{M}, \tag{8}$$

$$y_N = \frac{\alpha_B}{2\pi} + \left\lfloor -\frac{\alpha_B}{2\pi\Delta E}\right\rfloor \Delta E, \tag{9}$$

$$|y_0| = \min\{|y_N|, |y_P|\} = \min\{-y_N, \Delta E + y_N\} = -\left|y_N + \frac{\Delta E}{2}\right| + \frac{\Delta E}{2}, \tag{10}$$

where "gcd(M,N)" stands for greatest common divisor of M and N and $\{x\} = x - \lfloor x\rfloor$ denotes the fractional part with $\lfloor\cdot\rfloor$ denoting the floor function. The relative error of $f_{max,Rat}$ is of fourth order respective to α_B when compared to the exact solution of (5) (cf. Figure 7).

Proof. Considering that $\cos t$ and $\cos \Omega_B t + \alpha_B$ have large values, when their arguments are close to $2\pi k$ and $2\pi l$ with any $k, l \in \mathbb{Z}$, it is sufficient to examine how close the line

$$l(x) = \Omega_B x + \frac{\alpha_B}{2\pi} \tag{11}$$

gets to an integer-valued grid point, (k, l), on the plane. As all the integer-valued coordinate points are important, the line can be mapped to the surface of the unit torus by mapping [26]

$$T = \begin{cases} \mathbb{R}\times\mathbb{R} & \to S^1 \times S^1 \\ (x,y) & \to (\{x\},\{y\}), \end{cases} \tag{12}$$

thus, reducing the number of integer-valued coordinates to one, that is, the origin. The line (11) gets wound up on the surface of the torus and fills the surface densely in the case of irrational Ω_B, passing arbitrarily close to the origin and resulting in $f_{\text{sup}} = A + B$.

The situation becomes different if $f(t)$ becomes periodic owing to $\Omega_B \in \mathbb{Q}$. In this case, the mapped line $T(x, l(x))$ repeats itself in each period, leaving empty spaces on the surface of the torus. When the surface of the torus is cut along $x = 0$ and $y = 0$ and flattened out to represent it in the plane, $T(x, l(x))$ exhibits a family of parallel lines (cf. Figure 1). The equations of the whole family of lines can be defined as

$$C_k x + C_l y = C_0 + E_L, \tag{13}$$

where C_0 denotes a specific constant and E_L can take several values, indexed by $L \in \mathbb{Z}$, which identifies the line. As $l(x) = \Omega_B x + \frac{\alpha_B}{2\pi}$ is one of the aforementioned parallel lines, we consider E_L to take the value of 0 for this line, and thus, a link between the constants C_k, C_l, and C_0 can be defined as

$$C_0 = -\frac{\alpha_B}{2\pi\Omega_B} C_k, \tag{14}$$

$$C_l = -\frac{C_k}{\Omega_B}. \tag{15}$$

C_k can be selected freely. By setting $C_k = \Omega_B$, we obtain

$$C_0 = -\frac{\alpha_B}{2\pi}, \tag{16}$$

$$C_l = -1 \tag{17}$$

and Equation (13) becomes

$$\Omega_B x - l(x) = -\frac{\alpha_B}{2\pi} + E_L. \tag{18}$$

Applying T to $(x, l(x))$, we obtain

$$\Omega_B\{x\} - \{l(x)\} = -\frac{\alpha_B}{2\pi} + E_L, \tag{19}$$

$$\Omega_B\{x\} - \left\{\Omega_B x + \frac{\alpha_B}{2\pi}\right\} = -\frac{\alpha_B}{2\pi} + E_L, \tag{20}$$

$$\Omega_B(x - \lfloor x \rfloor) - \left(\Omega_B x + \frac{\alpha_B}{2\pi} - \left\lfloor \Omega_B x + \frac{\alpha_B}{2\pi} \right\rfloor\right) = -\frac{\alpha_B}{2\pi} + E_L, \tag{21}$$

$$-\Omega_B \lfloor x \rfloor + \left\lfloor \Omega_B x + \frac{\alpha_B}{2\pi} \right\rfloor = E_L. \tag{22}$$

Considering that $\Omega_B = N/M$, we obtain

$$\frac{-N\lfloor x \rfloor + M\lfloor \Omega_B x + \frac{\alpha_B}{2\pi} \rfloor}{M} = E_L. \tag{23}$$

As $\lfloor x \rfloor$ and $\lfloor \Omega_B x + \frac{\alpha_B}{2\pi} \rfloor$ are integer values, the smallest difference between two different values of the expression given in Equation (23) is

$$\Delta E = \frac{\gcd(M, N)}{M}. \tag{24}$$

Thus, the parallel lines are defined by

$$y(x, L) = \Omega_B x + \frac{\alpha_B}{2\pi} + L\Delta E, \qquad \text{with } L \in \mathbb{Z}. \tag{25}$$

Hence, (5) can be reformulated as

$$P_O: \qquad \max_{x,y,L} g_O(x, y) = A\cos 2\pi x + B\cos 2\pi y \tag{26}$$

$$\text{s.t.} \qquad y = \Omega_B x + \frac{\alpha_B}{2\pi} + L\Delta E, \qquad \text{with } x, y \in [0, 1), L \in \mathbb{Z}. \tag{27}$$

Figure 1a shows the equivalent representation of (5).

In the current form, the reformulated problem, that is, P_O is still impossible to solve in an analytically closed form, just as the original problem was. Therefore, instead of determining the exact solution, we settle for an estimation by expanding $g_O(x, y)$ into a Taylor series in the vicinity of the origin up to the third order, which leads to

$$P_T: \qquad \max_{x,y,L} g_T(x, y) = A(1 - 2\pi^2 x^2) + B(1 - 2\pi^2 y^2) \tag{28}$$

$$\text{s.t.} \qquad y = \Omega_B x + \frac{\alpha_B}{2\pi} + L\Delta E, \qquad \text{with } x, y \in [0, 1), L \in \mathbb{Z}. \tag{29}$$

Once L_O is determined, which determines the position of the line passing closest to the origin, condition (29) can be applied to objective (28) to simplify the problem to obtain

$$\left.\frac{\mathrm{d}g_T(x, y(x, L_O))}{\mathrm{d}x}\right|_{\tilde{x}} \overset{!}{=} 0. \tag{30}$$

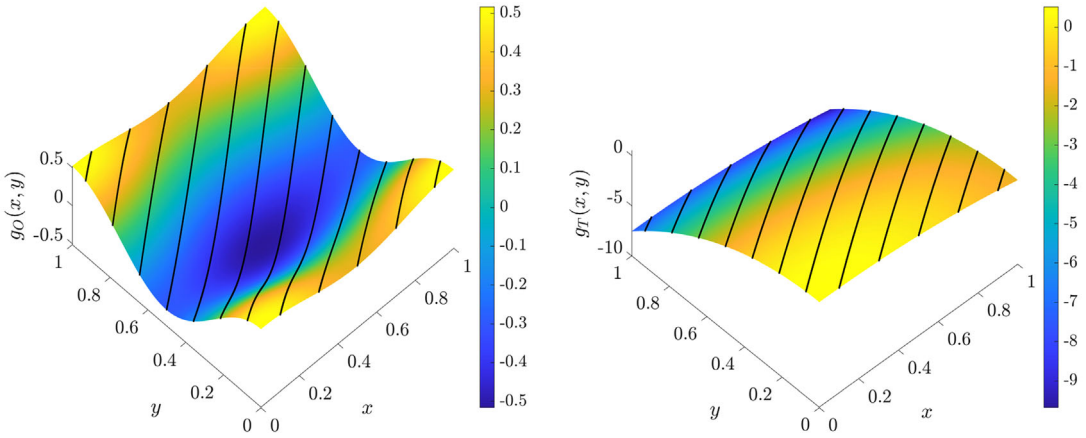

(a) The largest value of $g_O(x, y)$ taken along the line segments is $f_{\max}$.

(b) Approximation of $g_O(x, y)$ based on the third-order Taylor expansion in the vicinity of the origin, $g_T(x, y)$.

FIGURE 1 Periodic line on the surface of the unit torus. For visualization purposes, the torus has been cut and flattened out on the plane. $T(x, l(x))$ defines a family of lines in the form of $y = \Omega_B x + \frac{\alpha_B}{2\pi} + L\Delta E$.

The intercept of the line below and above the origin is defined as

$$y_N = \frac{\alpha_B}{2\pi} + L_N \Delta E, \tag{31}$$

$$y_P = \frac{\alpha_B}{2\pi} + (L_N + 1)\Delta E, \tag{32}$$

with

$$L_N = \left\lfloor -\frac{\alpha_B}{2\pi\Delta E} \right\rfloor. \tag{33}$$

Now, assume we know whether the upper or bottom line is closer to the origin, and write its equation as

$$y = \Omega_B x + y_0, \tag{34}$$

where y_0 is either y_N or y_P. Then, by evaluating (30), we obtain

$$4\pi^2 A x + 4\pi^2 B y \left.\frac{\mathrm{d}y}{\mathrm{d}x}\right|_{\tilde{x}} = 0, \tag{35}$$

$$A\tilde{x} + B(\Omega_B \tilde{x} + y_0)\Omega_B = 0, \tag{36}$$

which yields

$$\tilde{x} = -\frac{B\Omega_B y_0}{A + B\Omega_B^2}, \tag{37}$$

$$\tilde{y} = \frac{A y_0}{A + B\Omega_B^2}. \tag{38}$$

The values of $\tilde{x}$ and $\tilde{y}$ are applied again to the objective function $g_T(x, y)$, resulting in

$$f_{\max,\mathrm{T}} = A\left(1 - 2\pi^2\left(\frac{B\Omega_B y_0}{A + B\Omega_B^2}\right)^2\right) + B\left(1 - 2\pi^2\left(\frac{A y_0}{A + B\Omega_B^2}\right)^2\right) \tag{39}$$

$$= A\left(1 - 2\pi^2\left(\frac{B\Omega_B}{A + B\Omega_B^2}\right)^2 |y_0|^2\right) + B\left(1 - 2\pi^2\left(\frac{A}{A + B\Omega_B^2}\right)^2 |y_0|^2\right), \tag{40}$$

where the last equality is caused by the symmetry of the square function. Thus, the missing value of $|y_0|$ can be determined by

$$|y_0| = \min\{|y_N|, |y_P|\}, \tag{41}$$

$$= \min\{-y_N, \Delta E + y_N\}, \tag{42}$$

$$= -\left|y_N + \frac{\Delta E}{2}\right| + \frac{\Delta E}{2}. \tag{43}$$

Thus, a closed formula for the approximation of the maximum of the function $f(t)$ has been obtained. As $g_O(x, y)$ was expanded in the Taylor series up to the third order, the estimation error with respect to the exact solution is of fourth-order accuracy respective to α_B. □

Corollary 1. *The global minimum of $f(t) = A\cos t + B\cos(\Omega_B t + \alpha_B)$ can be found by reformulating the problem as*

$$\min_t f(t) = -\max_t(-f(t)) \tag{44}$$

$$= -\max_t(-A\cos(t) - B\cos(\Omega_B t + \alpha_B)), \tag{45}$$

$$= -\max_t(A\cos(t + \pi) + B\cos(\Omega_B t + \alpha_B + \pi)), \tag{46}$$

$$= -\max_{\tilde{t}}(A\cos(\tilde{t}) + B\cos(\Omega_B \tilde{t} + \underbrace{\alpha_B + (1 - \Omega_B)\pi}_{=:\tilde{\alpha}_B})). \tag{47}$$

Thus, the minimization problem is converted back to the previous maximization problem.

Corollary 2. *The estimate $f_{max} \approx f_{sup,Irr} = A + B$ can be obtained using the aforementioned method if the Taylor series expansion of $g_O(x, y)$ is stopped after obtaining the first-order term, leading to $g_O(x, y) \approx A + B$. Hence, the relative error of the estimate $f_{sup,Irr}$ with respect to the exact solution of the maximization problem (5) is of the second order respective to α_B (c.f. Figure 7).*

Remark 1. To obtain a more accurate result ($\epsilon_{\text{rel}} = \mathcal{O}(\alpha_B^6)$, cf. Figure 7), the solution $(\tilde{x}, \tilde{y})$ can be substituted back into $g_O(x, y)$, instead of $g_T(x, y)$, yielding

$$f_{\max,\text{T}} = A\cos\left(-2\pi\frac{B\Omega_B y_0}{A + B\Omega_B^2}\right) + B\cos\left(2\pi\frac{Ay_0}{A + B\Omega_B^2}\right) \tag{48}$$

$$= A\cos\left(2\pi\frac{B\Omega_B}{A + B\Omega_B^2}|y_0|\right) + B\cos\left(2\pi\frac{A}{A + B\Omega_B^2}|y_0|\right), \tag{49}$$

where the last equality is caused by the evenness of the cosine function.

3 | SBs OF ESCAPE FROM AN ASYMMETRICALLY TRUNCATED QUADRATIC POTENTIAL WELL UNDER HARMONIC EXCITATION

3.1 | Problem setting

As we have derived a sufficiently accurate method for the estimation of the minimum and maximum values of the sum of two harmonics, we can proceed to apply the results to the problem of escape from an asymmetrically truncated quadratic potential well under harmonic excitation. The equation of motion is defined as

$$m\ddot{x} + mV'(x) = F\sin(\Omega_x \tau + \beta), \tag{50}$$

$$x(0) = \tilde{x}_0, \tag{51}$$

$$\dot{x}(0) = \tilde{u}_0, \tag{52}$$

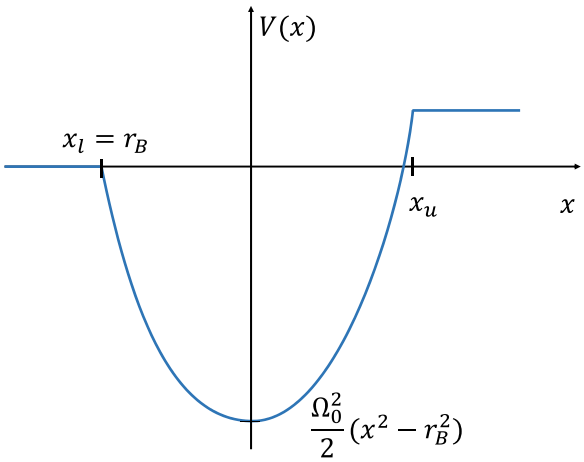

FIGURE 2 Asymmetrically truncated quadratic potential $V(x)$

with

$$V(x) = \begin{cases} -\frac{\Omega_0^2}{2} r_B^2 + \frac{\Omega_0^2}{2} x^2 & \text{for } x_l \le x \le x_u, \\ \frac{-r_B^2 + x_l^2}{2} \Omega_0^2 & \text{for } x < x_l, \\ \frac{-r_B^2 + x_u^2}{2} \Omega_0^2 & \text{for } x_u < x, \end{cases} \tag{53}$$

where Ω_x denotes the frequency, β denotes the initial phase, and F denotes the amplitude of excitation. Ω_0 denotes the natural frequency of the potential well and m denotes the mass of the particle. The boundary of the potential on the left from the origin is located at $x_l \in (-\infty, 0)$ and from the right at $x_u \in (0, \infty)$. We define

$$r_B := \min\{-x_l, x_u\} \tag{54}$$

as the distance between the deepest point of the potential to the closer boundary. Figure 2 shows the potential with its characteristic quantities.

Considering the non-dimensional time $t := \Omega_0 \tau$, excitation amplitude $f := \frac{F}{m}$, and excitation frequency $\omega := \frac{\Omega_x}{\Omega_0}$, the equation of motion can be reformulated as

$$\ddot{x} + \tilde{V}'(x) = f \sin(\omega t + \beta), \tag{55}$$

$$x(0) = x_0 := \tilde{x}_0, \tag{56}$$

$$\dot{x}(0) = u_0 := \frac{\tilde{u}_0}{\Omega_0}, \tag{57}$$

with

$$\tilde{V}(x) = \begin{cases} -\frac{r_B^2}{2} + \frac{x^2}{2} & \text{for } x_l \le x \le x_u, \\ \frac{-r_B^2 + x_l^2}{2} & \text{for } x < x_l, \\ \frac{-r_B^2 + x_u^2}{2} & \text{for } x_u < x. \end{cases} \tag{58}$$

3.2 | Escape definitions and analytical solution of the particle motion in the well

Possibly, the most intuitive definition one associates with escape from a potential, which has its minimum at $x = 0$, is that "if $\exists t_0$ such that $|x(t)| > R_B > 0, \forall t > t_0$, where R_B is a suitably defined positive constant (e.g., $R_B := \max\{-x_l, x_u\}$), the particle escapes from the well." In other words, the particle escapes if after a certain time point it never returns to the vicinity of the bottom of the potential well. This definition, however, does not facilitate numerical investigations, as the solution has to be calculated for all times.

As an alternative, for numerical purposes, the following escape criterion can be considered: "If $|x(t)| \geq R_B$ for any $t \geq 0$, the particle escapes." Here, R_B is selected such that it is greater than or equal to the furthest potential boundary. This criterion means that for escape it is sufficient that the particle leaves the potential well once. (Actually, it means that it can later return!) If there is no well-defined potential boundary (e.g., gravitational potential of a mass), a sufficiently large value of R_B often works well.

For analytical purposes, this definition might be complex, especially in the given case with $\tilde{V}(x)$, where the evaluation of the piecewise-defined potential is not possible without case distinction. Thus, to overcome this difficulty, for analytical purposes, the following escape criterion is used in the current paper: "if

$$(x(t) - x_l)(x_u - x(t)) \leq 0 \tag{59}$$

for any $t \geq 0$, then the particle escapes." We observe that for small excitation amplitudes, this criterion is accurate; however, for large values of F, the non-linearity of the potential field will result in appearing of fundamentally different escape behaviors (see Figures 10 and 11).

Owing to the escape condition (59), the movement has to be calculated for $x_l < x < x_u$ values. Thus, the differential equation becomes linear, and an explicit analytic solution for $\omega \neq 1$ (otherwise resonance and escape for any IC) can be defined as

$$x(t) = R\sin(t + \alpha) + P\sin(\omega t + \beta), \tag{60}$$

with

$$P = \frac{f}{1 - \omega^2}, \tag{61}$$

$$R = \sqrt{(x_0 - P\sin\beta)^2 + (u_0 - P\omega\cos\beta)^2}, \tag{62}$$

$$\alpha = \operatorname{atan2}(x_0 - P\sin\beta, u_0 - P\omega\cos\beta). \tag{63}$$

3.3 | Estimation of the non-escaping set in the IC plane for quasi-periodic motions

The ratio of the excitation frequency and natural frequency of the potential well significantly affects the periodicity of the motion. In ref. [27], the simpler case $\omega \in \mathbb{R}\backslash\mathbb{Q}$ (when the motion is quasi-periodic) was investigated thoroughly. The supremum of the absolute displacement $r_{\text{sup}} := \max_t |x(t)|$ can be accurately estimated by

$$r_{\text{sup}} = R + |P|. \tag{64}$$

The values of $|P|$ and R from Equations (61) and (62) can be substituted into Equation (64), and by demanding $r_{\text{sup}} \leq r_B$ for the non-escaping scenario, we obtain

$$r_B \geq R + |P|, \tag{65}$$

$$r_B - |P| \geq R. \tag{66}$$

Therefore, for $|P| > r_B$, no set of points fulfilling the inequality exists, as R is a non-negative number. Thus, based on this estimation, for

$$f > r_B|1 - \omega^2|, \tag{67}$$

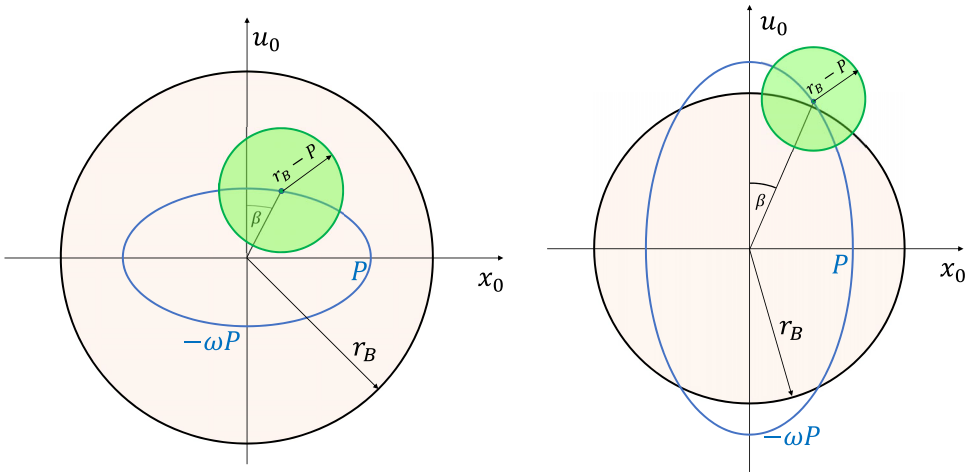

FIGURE 3 SB location, D_P on the $x_0 - u_0$ plane

the particle escapes from the well for any IC. However, if $|P| \leq r_B$, both sides can be squared in Equation (66), and we obtain

$$D_P : \qquad (r_B - |P|)^2 \geq (x_0 - P\sin\beta)^2 + (u_0 - P\omega\cos\beta)^2. \tag{68}$$

This inequality defines the closed circular disk centered at $(P\sin\beta, P\omega\cos\beta)$ with radius $R_D = r_B - |P|$.

The disk with the largest area is obtained for $|P| = 0$, i.e., $F = 0$, which implies no external excitation, i.e., the non-escaping set due to initial conditions only. Then, it is a disk with radius r_B

$$D_0 : \qquad r_B^2 \geq x_0^2 + u_0^2, \tag{69}$$

at the origin, having a total area of

$$A_0 = \pi r_B^2. \tag{70}$$

There is a significant difference between $\omega < 1$ and $\omega > 1$. In the first case, for any admissible $|P|$, the circular disk defined by Equation (68) stays within D_0; however, in the second case, a fraction or the total area of the disk D_P can lie outside of D_0. These two cases of the non-escaping set are shown in Figure 3.

In both cases, the total area of the SB, also referred to as global integrity measure (GIM), is

$$A_P = \pi(r_B - |P|)^2. \tag{71}$$

Although these observations with regard to the area of the SB might be trivial, they are considered to be important for practical purposes, as the ICs of the particle cannot be controlled with very high accuracy. It is important to have a reference case to which the results can be compared while investigating the non-escaping sets of ICs from non-quadratic potentials. Knowing the dependence of the global integrity measure on the parameters of the system and excitation, the benchmark case of the truncated quadratic potential can characterize other potentials with regard to their erosion characteristics.

3.4 | Estimation of the non-escaping set in the IC plane for $N : M$ excitation

We have determined the mathematical relation between the parameters of our system and location and size of the SBs in the plane of the ICs with regard to the irrational ratio of the excitation and natural frequencies of the potential well. Hereafter, we focus on the case where this ratio is rational, i.e., $\omega = \frac{N}{M}$.

Equation (60) defines $x(t; x_0, u_0, f, \omega, \beta)$ as a function of the time, depending on several parameters. Reinterpreting the role of parameters and variables, we can define Equation (60) as $x(t, x_0, u_0; f, \omega, \beta)$, a function of three variables, the time

and ICs of position and velocity. Finding

$$x_{\min}(x_0, u_0) := \min_{\tilde{t}\geq 0} x(\tilde{t}, x_0, u_0) \tag{72}$$

and

$$x_{\max}(x_0, u_0) := \max_{\tilde{t}\geq 0} x(\tilde{t}, x_0, u_0) \tag{73}$$

respectively, we obtain the maximum negative and positive displacements as a function of two variables for a given choice of the remaining parameters. The escape condition (59) can be evaluated, and the SBs are defined by

$$SB: \quad (x_l < x_{\min}(x_0, u_0)) \quad \cap \quad (x_{\max}(x_0, u_0) < x_u). \tag{74}$$

To determine $x_{\max}(x_0, u_0)$ based on Theorem 1, the optimization problem

$$\max_{\tilde{t}\geq 0} x(\tilde{t}) = \max_{\tilde{t}\geq 0}(R\sin(\tilde{t}+\alpha) + P\sin(\omega\tilde{t}+\beta)), \tag{75}$$

can be rewritten in the standard form

$$\max_{t\geq 0} x(t) = \max_{t\geq 0}(R\cos t + P\cos(\omega t + \alpha_{B,\max})) \tag{76}$$

with the transformation

$$t = \tilde{t} + \alpha - \frac{\pi}{2}. \tag{77}$$

Then, the new phase shift is defined as

$$\alpha_{B,\max} = \frac{\pi}{2}(\omega - 1 + 2\sigma(-P)) - \omega\alpha + \beta \tag{78}$$

with the Heaviside function

$$\sigma(x) = \begin{cases} 1 & x \geq 0, \\ 0 & x < 0, \end{cases} \tag{79}$$

which has to be applied to consider the case $P < 0$. We can find $x_{\min}(x_0, u_0)$ by applying Corollary 1 to Equation (60)

$$x_{\min}(x_0, u_0) = -\max_{\tilde{t}\geq 0}(R\sin(\tilde{t}+\alpha+\pi) + P\sin(\omega\tilde{t}+\beta+\pi)), \tag{80}$$

and subsequently transforming it into the standard form, that is,

$$x_{\min}(x_0, u_0) = -\max_{t\geq 0}(R\cos t + |P|\cos(\omega t + \alpha_{B,\min})), \tag{81}$$

using

$$t = \tilde{t} + \alpha + \frac{\pi}{2}, \tag{82}$$

$$\alpha_{B,\min} = \frac{\pi}{2}(1 - \omega + 2\sigma(-P)) - \omega\alpha + \beta. \tag{83}$$

Applying the results of Theorem 1, we obtain the estimate

$$\hat{x}_{\max}(x_0, u_0) = R(1 - 2\pi^2\tilde{x}_{\max}^2) + |P|(1 - 2\pi^2\tilde{y}_{\max}^2), \tag{84}$$

$$\hat{x}_{\min}(x_0, u_0) = -R(1 - 2\pi^2\tilde{x}_{\min}^2) - |P|(1 - 2\pi^2\tilde{y}_{\min}^2), \tag{85}$$

or even more accurately

$$\hat{x}_{\max}(x_0, u_0) = R\cos(2\pi\tilde{x}_{\max}) + |P|\cos(2\pi\tilde{y}_{\max}), \tag{86}$$

$$\hat{x}_{\min}(x_0, u_0) = -R\cos(2\pi\tilde{x}_{\min}) - |P|\cos(2\pi\tilde{y}_{\min}), \tag{87}$$

with

$$\tilde{x}_{\max/\,\min} = \frac{\omega|P||y_{0,\max/\,\min}|}{R + \omega^2|P|}, \tag{88}$$

$$\tilde{y}_{\max/\,\min} = \frac{R|y_{0,\max/\,\min}|}{R + \omega^2|P|}, \tag{89}$$

$$|y_{0,\max/\,\min}| = -\left|y_{N,\max/\,\min} + \frac{\Delta E}{2}\right| + \frac{\Delta E}{2}, \tag{90}$$

$$y_{N,\max/\,\min} = \frac{\alpha_{B,\max/\,\min}}{2\pi} + L_{0,\max/\,\min}\Delta E, \tag{91}$$

$$L_{0,\max/\,\min} = \left\lfloor -\frac{\alpha_{B,\max/\,\min}}{2\pi\Delta E} \right\rfloor, \tag{92}$$

$$\Delta E = \frac{\gcd(M, N)}{M}, \tag{93}$$

where the indexing notation "max\min" has been introduced to simultaneously denote both cases for brevity. The difference in the functions $\hat{x}_{\max}(x_0, u_0)$ and $\hat{x}_{\min}(x_0, u_0)$ results from the distinct values of $\alpha_{B,\max}$ and $\alpha_{B,\min}$. Without the loss of generality, M and N can be chosen to be relative primes; thus, $\Delta E = \frac{1}{M}$, and Equations (90) to (92) can be simplified as

$$|y_{0,\max}(\alpha_{B,\max/\,\min})| = -\left|\frac{\alpha_{B,\max/\,\min}}{2\pi} - \frac{1}{M}\left\lfloor\frac{M\alpha_{B,\max/\,\min}}{2\pi}\right\rfloor - \frac{1}{2M}\right| + \frac{1}{2M}. \tag{94}$$

For any point (x_0, u_0) in SB, it simultaneously holds that $(x_0, u_0) \in SB_u$ and $(x_0, u_0) \in SB_l$; thus, $(x_0, u_0) \in SB_u \cap SB_l$ with $SB_u := \{(x_0, u_0) \in SB_u | \hat{x}_{\max}(x_0, u_0) < x_u\}$ and $SB_l := \{(x_0, u_0) \in SB_l | x_l < \hat{x}_{\min}(x_0, u_0)\}$. It is the intersection of both sublevel sets. The analytical determination of the boundary of the intersection is very intricate (cf. Figure 4a and 4c); however, special cases appear (cf. Figure 4c and 4d) when the complexity is significantly reduced, that is, in the case of a symmetric potential ($-x_l = x_u$) and in the case of $SB_l \subseteq SB_u$ (or $SB_u \subseteq SB_l$) for all the values of f and β. If $N + M$ is an even number, we possess the latter case, as Equation (94) is periodic in $\frac{2\pi}{M}$, that is,

$$|y_{0,\max}(x)| = \left|y_{0,\max}\left(x + \frac{2\pi}{M}\right)\right|, \tag{95}$$

and by calculating

$$\alpha_{B,\max} - \alpha_{B,\min} = (\omega - 1)\pi = \frac{N - M}{M}\pi \tag{96}$$

we determine the aforementioned periodicity; thus, $x_{\max}(x_0, u_0) \equiv x_{\min}(x_0, u_0)$ for $N + M$ even. Hereafter, an analytical estimate for the boundary of the SB is given for the aforementioned two cases.

3.4.1 | $|x_l| \gg x_u$ or $N + M$ even

If one of the potential boundaries lies much further from the center of the well as the other one, the particle will escape towards the closer boundary; thus, in this case, the level set corresponding to the closer boundary is considered to be important.

Without loss of generality, we can assume $|x_l| \gg x_u$; thus, $SB_u \subseteq SB_l$ (otherwise the same calculation is performed with $\hat{x}_{\min}(x_0, u_0)$). The size of the SBs depends on three parameters only, that is, f, M, and N, as it transpires that β is only a

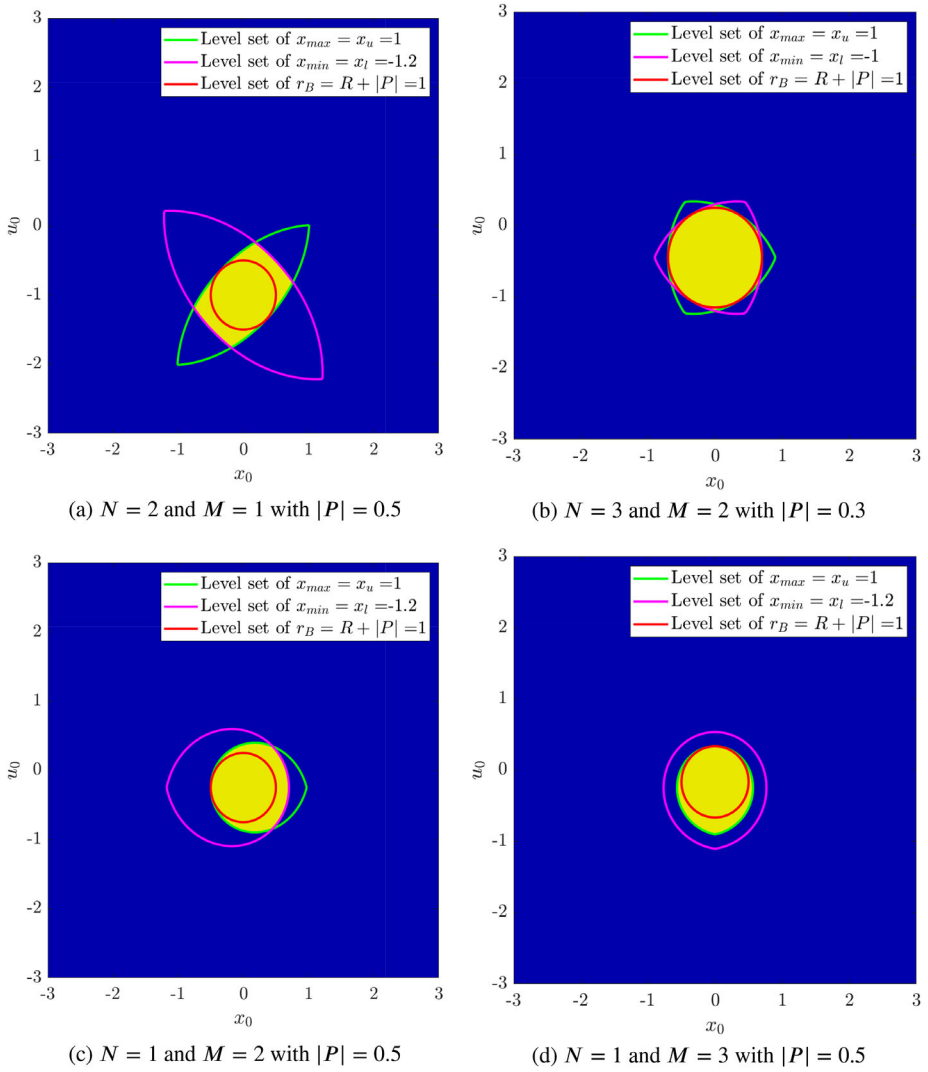

FIGURE 4 Analytically obtained estimate for the SB with regard to escape in the plane of the ICs for different values of the excitation frequency $\omega = \frac{N}{M}$. The level sets of $x_{\max}(x_0, u_0) = x_u$ and $x_{\min}(x_0, u_0) = x_l$ are depicted with green and pink, respectively. The circular disk defined by Equation (68) is shown in red. The intersection of the interiors of the level sets (SB_u and SB_l) defines the non-escaping region SB (in yellow).

rotation in the IC plane. To gain some understanding with regard to the shape of the SBs, we apply the escape condition (59) to the less accurate but mathematically manageable estimate (84), resulting in

$$\hat{x}_{\max}(x_0, u_0) = R + |P| - \frac{2\pi^2 R|P||y_{0,\max}|^2}{R + \omega^2|P|} \stackrel{!}{=} x_u. \tag{97}$$

As only R and $|y_{0,\max}|$ depend on x_0 and y_0 (cf. Equation (62) and (63)), we can determine a function in polar coordinates, centered at $(P\sin\beta, P\omega\cos\beta)$, which describe the distance of the boundary depending on the angle, $R(\varphi)$. To obtain this relation, $|y_{0,\max}|$ can be redefined as

$$g(\varphi; M, N) := |y_{0,\max}(\varphi)| = -\left|\frac{N}{M}\frac{\varphi}{2\pi} - \frac{1}{M}\left\lfloor\frac{N\varphi}{2\pi}\right\rfloor - \frac{1}{2M}\right| + \frac{1}{2M} \tag{98}$$

with

$$\varphi := -\frac{\alpha_{B,\max}}{\omega} = \alpha - \frac{\beta}{\omega} - \frac{\pi}{2\omega}(\omega - 1 + 2\sigma(-P)), \tag{99}$$

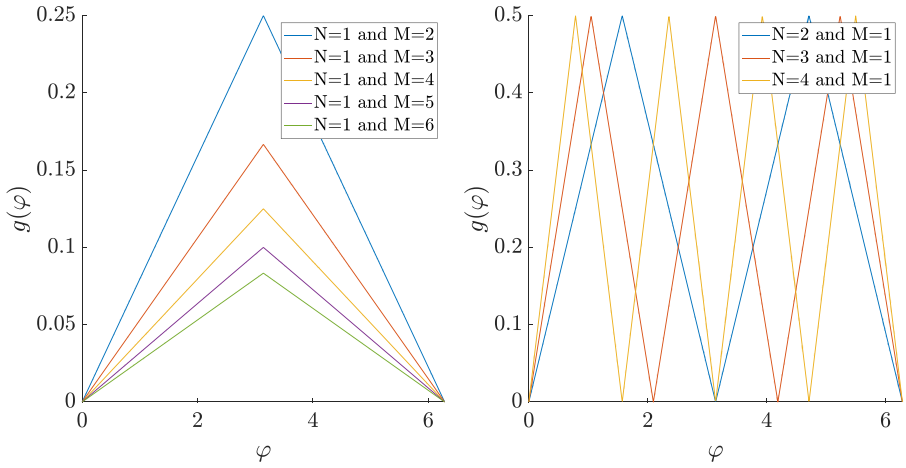

(a) $N = 1$, $M = 1, 2, 3, \ldots$ (b) $N = 1, 2, 3, 4$, $M = 1$

FIGURE 5 Triangle wave function $g(\varphi; M, N)$ for different values of M and N

being the 2π periodic angle coordinate. Equation (98) defines a triangle wave with period $\frac{2\pi}{N}$, amplitude $\frac{1}{4M}$, and a positive offset of $\frac{1}{4M}$.

Equation (97) inserted into escape condition (59) can be rewritten as

$$R^2 + \big((\omega^2 + 1 - 2\pi^2 g^2(\varphi))|P| - x_u\big)R + \omega^2|P|(|P| - x_u) = 0 \tag{100}$$

and solved for R resulting in

$$R(\varphi) = \frac{x_u - \big(1 + \omega^2 - \pi^2 g^2(\varphi)\big)|P|}{2} \pm \frac{\sqrt{4g^4(\varphi)\pi^4|P|^2 - 4\pi^2((\omega^2+1)|P| - x_u)|P|g^2(\varphi) + \big((\omega^2-1)|P| - x_u\big)^2}}{2}, \tag{101}$$

where for $|P| < x_u$, one of the roots is positive and the other one is negative, thus uniquely determining the boundary of the SB by the positive root (cf. green curve in Figure (6a)).

For $\varphi = \frac{n}{2\pi}$ with $n = 0 \ldots N-1$, we have $g(\varphi) = 0$ and the solution becomes $R = x_u - |P|$, implying that at this point, the boundary of the SB defined in Equation (97) touches the circle defined in Equation (68) (cf. Figure 4).

For $\varphi \neq \frac{n}{2\pi}$ with $n = 0 \ldots N-1$, we have $R(\varphi) > x_u - |P|$ implying that the circle is the inscribed circle of the SB. An exception occurs when $N = 1$. In this case an SB can exist even for $x_u < |P|$. This means that the amplitude of the particular solution $|P|$ can be greater than x_u without leading to escape for certain initial conditions. We denote the highest value of P beyond which no SB exists by P_{crit}. For $x_u < |P| < P_{\text{crit}}$ the circle defined in Equation (68) does not exist anymore and the origin of the polar coordinate system $(x_0, u_0) = (P\sin\beta, P\omega\sin\beta)$ shifts outside the SB; thus, for some values of φ we find $R_{1,2}(\varphi) < 0$, which is physically meaningless; however, for the rest of φ, two positive roots $R_{1,2}(\varphi)$ exist, thus defining the SB (cf. blue curve in Figure (6a)).

It is possible to derive an upper estimate for P_{crit}, considering that when SBs disappear, the expression under the square root in Equation (101) just becomes zero. At this moment, the SB has shrunk to a point along the direction of the angle $\varphi = \pi$, where $g(\varphi)$ takes its maximum resulting in $g(\varphi) = \frac{1}{2M}$ (Figure 5). Considering that $N = 1$ in the current situation, we have $\omega = \frac{1}{M}$. Using these observations, the discriminant of Equation (100)

$$\big(\omega^2 + 1 - 2\pi^2 g^2(\varphi))|P| - x_u\big)^2 - 4\big(\omega^2|P|^2 - x_u|P|\omega^2\big) \stackrel{!}{=} 0 \tag{102}$$

vanishes for

$$P_{\text{crit}} = \frac{2\Big(2M^2 - 2\sqrt{2}\,\pi - \pi^2 - 2\Big)M^2}{(2M^2 - \pi^2 + 4M + 2)(2M^2 - \pi^2 - 4M + 2)}x_u. \tag{103}$$

In Figure 8, the values of $\frac{P_{\text{crit}}}{x_u}$ are depicted for $N = 1$ and $M = 2 \ldots 10$.

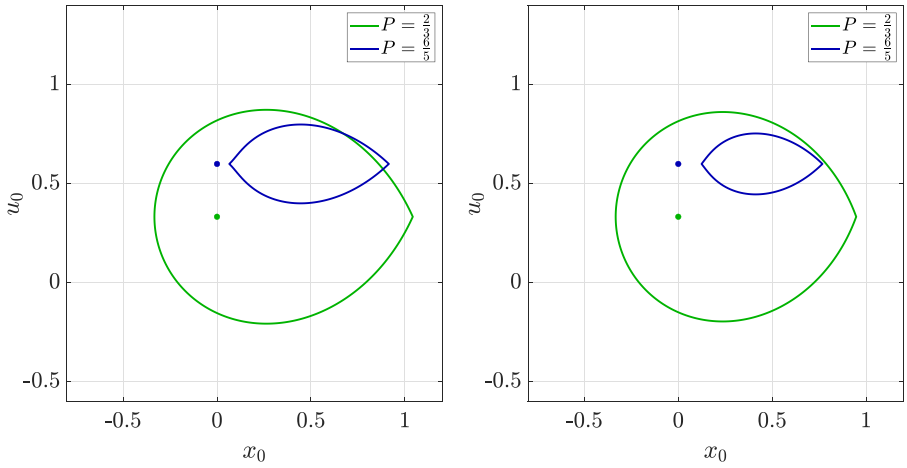

(a) Using estimate in Eq. (84) (b) Using estimate in Eq. (86)

FIGURE 6 Boundary of the SBs in the plane of the ICs for $\omega = \frac{N}{M} = \frac{1}{2}$, $\beta = 0$, $x_l = -\infty$, and $x_u = 1$ for different values of P using the estimates defined in Equations (84) and (86). For $P > x_u$ (blue curve), an SB still exists. The dots represent the origin of the polar coordinates $(P\sin\beta, P\omega\cos\beta)$, in which the curve is defined by Equation (101). The estimates of the SBs on the left are greater owing to $g_T(x_0, u_o) \leq g_O(x_0, u_o)$.

For $N \geq 2$, the aforementioned augmentation of $P_{\text{crit}} > x_u$ cannot take place, as it would indicate the existence of the N pieces of disjoint non-escaping basins (caused by the N-fold rotational symmetry) centered around the point $(P\sin\beta, P\omega\cos\beta)$; therefore, in these cases, the analytically predicted SB disappears if $|P| > 1$.

To analytically estimate the area enclosed by the level set $x_{\max}(x_0, u_0) = x_u$, the following integral has to be evaluated:

$$A_{\max} = \int_0^{2\pi} \frac{R^2(\varphi)}{2} \mathrm{d}\varphi, \tag{104}$$

which, due to the N-fold rotational and mirror symmetry, can be reduced to

$$A_{\max} = N \int_0^{\frac{\pi}{N}} R^2(\varphi) \mathrm{d}\varphi. \tag{105}$$

Equation (105) results in elliptic integrals, which require lengthy calculation; however, to provide an estimate, the Taylor expansion of $R^2(\varphi)$ can be used. Calculating it around $\varphi = 0$ up to the fifth order, we obtain

$$R^2(\varphi) = (x_u - |P|)^2 + \frac{(x_u - |P|)^2 |P| \omega^2}{|P|(\omega^2 - 1) + x_u} \varphi^2 + \frac{(x_u - |P|)^2 |P|^2 \left((3\omega^2 - 1)|P| + x_u\right)\omega^4}{4\left((\omega^2 - 1)|P| + x_u\right)^3} \varphi^4 + \mathcal{O}(\varphi^6). \tag{106}$$

Performing integration and inserting $\omega = \frac{N}{M}$, we obtain

$$A_{\max,\mathrm{T}} = (x_u - |P|)^2 \pi \left(1 + \frac{\pi^2}{3\left(N^2 + M^2\left(\frac{x_u}{|P|} - 1\right)\right)} + \frac{\left(3N^2 + M^2\left(\frac{x_u}{|P|} - 1\right)\right)\pi^4}{20\left(N^2 + M^2\left(\frac{x_u}{|P|} - 1\right)\right)^3} \right). \tag{107}$$

Considering that $x_u > |P|$, denominators would always be positive; thus, for large values of N and M, the higher order terms of the expansion decrease and the SB converges to the circular disk determined in Subsection 3.3.

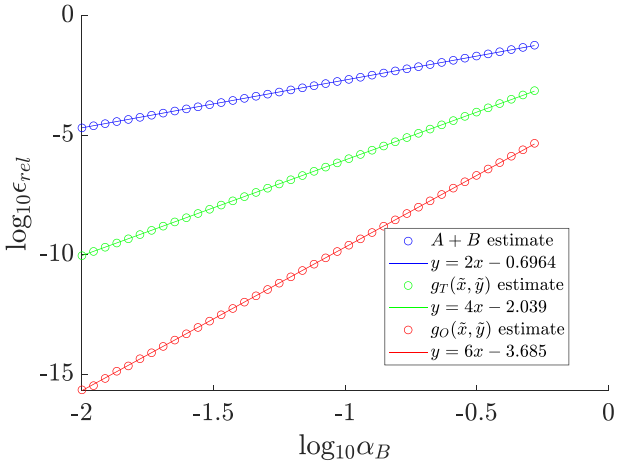

FIGURE 7 Logarithm of the relative error, $\epsilon_{\text{rel}} := \frac{|\hat{f}_{\max} - f_{\max}|}{f_{\max}}$ of the maximum value estimation depicted over the logarithm of $\alpha_B \in (0.01, \frac{\pi}{6})$ for $\max_{t\in(0,4\pi)} \cos(t) + \cos(\frac{1}{2}t + \alpha_B)$. The one-parameter line perfectly coincides with the numerically obtained data.

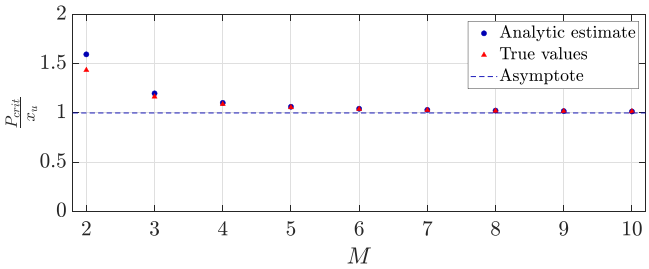

FIGURE 8 Convergence of $\frac{P_{\text{crit}}}{x_u}$ to 1 with an increase in the number of M for $N = 1$ held constant.

3.4.2 | $x_u = -x_l$ with $N + M$ odd

If the potential is symmetric and $N + M$ is an odd number, the SB possesses $2N$-fold rotational symmetry and mirror symmetry; thus, its area can be calculated by

$$A_{\max} = 2N \int_0^{\frac{\pi}{2N}} R^2(\varphi) \mathrm{d}\varphi. \tag{108}$$

Using the Taylor expansion of $R^2(\varphi)$ given in Equation (106), we obtain the value of

$$A_{\max,\mathrm{T}} = (x_u - |P|)^2 \pi \left(1 + \frac{\pi^2}{12\left(N^2 + M^2\left(\frac{x_u}{|P|} - 1\right)\right)} + \frac{\left(3N^2 + M^2\left(\frac{x_u}{|P|} - 1\right)\right)\pi^4}{320\left(N^2 + M^2\left(\frac{x_u}{|P|} - 1\right)\right)^3} \right). \tag{109}$$

Figure 9c shows an example for $N = 2$ and $M = 1$.

4 | COMPARISON WITH NUMERICAL RESULTS

In this section, the analytically obtained results are compared with numerical results for some choice of the parameters.

In Figure 7, the logarithm values of the relative errors of the maximum estimates given by Equations (6), (7), and (49)

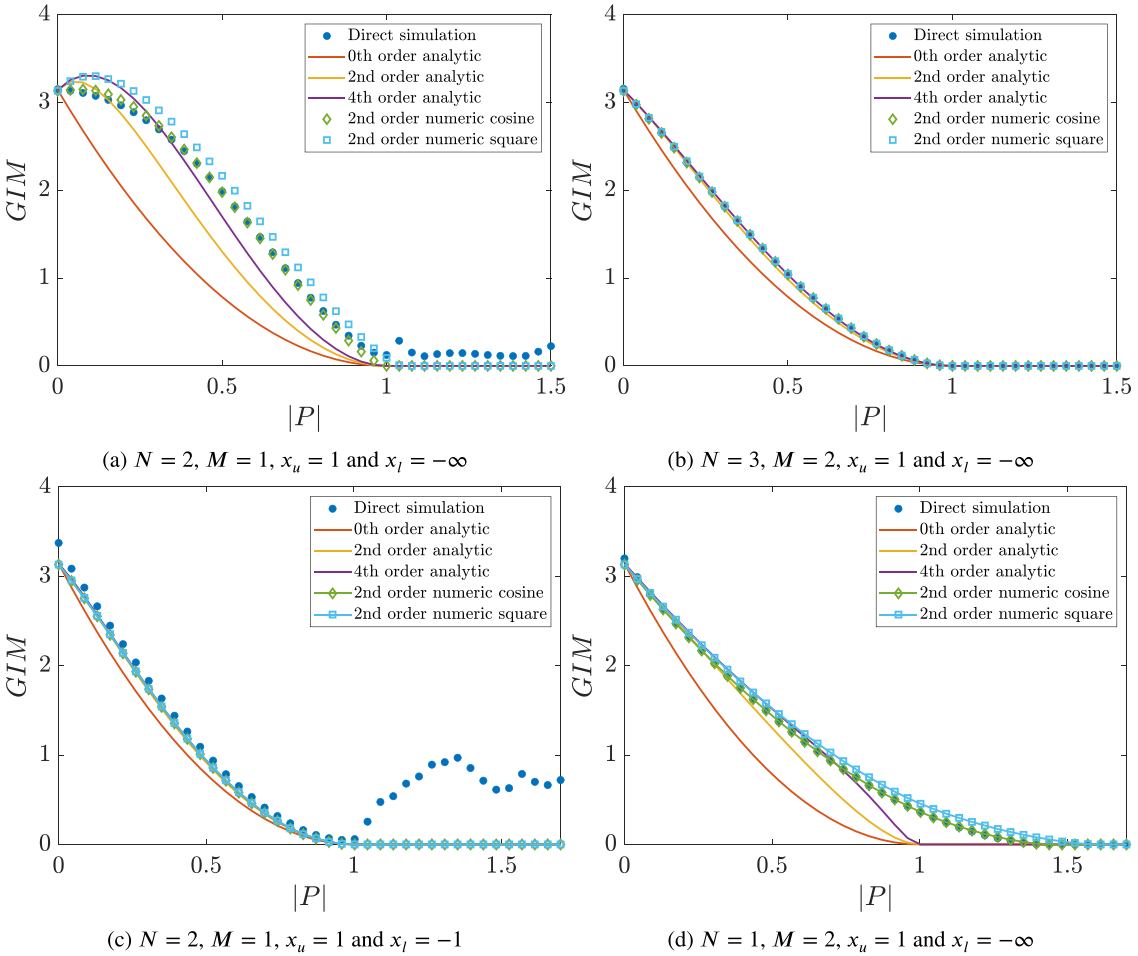

(a) $N = 2$, $M = 1$, $x_u = 1$ and $x_l = -\infty$

(b) $N = 3$, $M = 2$, $x_u = 1$ and $x_l = -\infty$

(c) $N = 2$, $M = 1$, $x_u = 1$ and $x_l = -1$

(d) $N = 1$, $M = 2$, $x_u = 1$ and $x_l = -\infty$

FIGURE 9 Global integrity measure (*GIM*) depending on the amplitude of the excitation for different values of the excitation frequency (deep blue dots). The red, yellow, and purple lines denote the analytic estimates based on Equation (107). The green diamonds and light blue squares denote the numerical integration of the area of the sublevel set defined by $\hat{x}_{\max(x_0,u_0)} < x_u$, where $\hat{x}_{\max(x_0,u_0)}$ is defined by Equations (86) and (84), respectively. Figure 7d shows that the Taylor expansion of Equation (101) can provide an estimate for $|P| < x_u$ only; however, the semi-analytic method depicted with green diamonds still generates accurate results.

are plotted over the logarithm of the phase shift, that is, α_B for

$$\max_{t\in(0,4\pi)} \cos(t) + \cos\left(\frac{1}{2}t + \alpha_B\right). \tag{110}$$

In the defined interval of $\alpha_B \in (0.01, \frac{\pi}{6})$, the relative error of estimates (6), (7), and (49) are quadratic, quartic, and of sixth order, respectively.

Figure 8 shows the estimates for the critical, re-scaled forcing value $\frac{|P|}{x_u}$ if $N = 1$ and $SB_u \subseteq SB_l$ (or vice versa) for different values of M. A comparison of Equation (107) to the direct numerical simulation and semi-analytic estimates, based on the numerical integration of the sublevel sets defined by $\hat{x}_{\max(x_0,u_0)} < x_u$, where $\hat{x}_{\max(x_0,u_0)}$ is given by Equation (86) and Equation (84), respectively, is shown in Figure 9. For the smallest possible values of M and N, that is, $N = 1$ and $M = 2$ or $N = 2$ and $M = 1$, the analytic estimates are not very accurate; however, for larger values of N and M, the estimates of the *GIM* become more and more accurate. The direct simulation shows that SBs exist, even for $|P| > x_u$; however, their prediction is not possible with the aforementioned method, as the escape condition (59) is restrictive: the particle leaves the potential in each period of excitation; however, owing to the large value of the excitation amplitude and essential non-linearity at the potential boundary, it returns to the well. For increasing values of the excitation amplitude, non-linear effects occur (cf. Figure 10 with quite smooth boundary and Figure 11 with fractal-like boundary and period tripling).

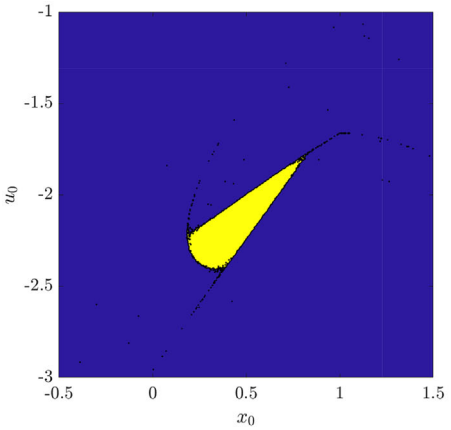

(a) SB on the IC plane.

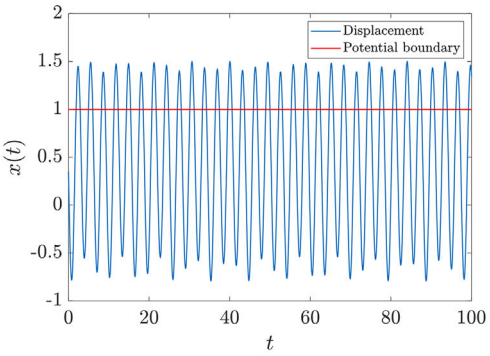

(b) Time evolution of the solution for $x_0 = 0.352$, $u_0 = -2.224$.

FIGURE 10 Wedge-shaped SB for $P_{\text{crit}} < |P| = 1.3$ with $N = 2$, $M = 1$, $x_1 = -\infty$, and $x_u = 1$. The direct integration was performed during 50 periods of the excitation. For the selected IC from the interior of the SB, the particle leaves the potential well in every period of the excitation; however, the exciting force is large enough to pull it back into the well; thus, an SB exists for supercritical forcing. The non-escaping mechanism is only possible for excitation frequencies above the natural frequency of the well, that is, $\omega > 1$. The prediction of these basins cannot be performed using the analytical method of this study.

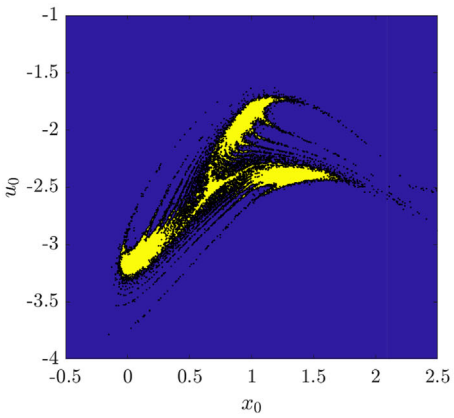

(a) SB on the IC plane.

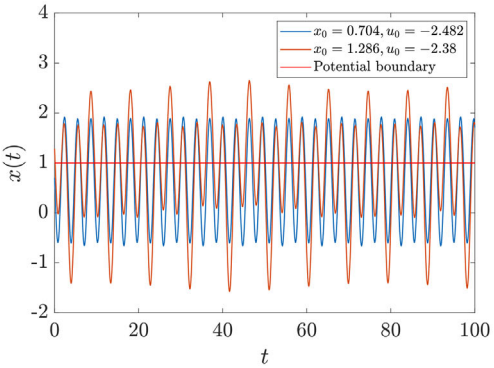

(b) Time evolution of the solution for $x_0 = 1.286$, $u_0 = -2.38$ and for $x_0 = 0.704$, $u_0 = -2.482$.

FIGURE 11 Fractal-like SB for $P_{\text{crit}} < |P| = 1.6$ with $N = 2$, $M = 1$, $x_1 = -\infty$, and $x_u = 1$. The direct integration was done during 100 periods of the excitation. Depending on the selection of the IC, the time evolution of the particle displacement is periodic-like, or it undergoes a periodic-tripling.

Figure 10 shows a wedge-shaped SB for supercritical forcing value $\frac{|P|}{x_u} = 1.3\,(N = 2, M = 1 \text{ and } x_l = -\infty)$, which cannot be predicted using the aforementioned model. However, the boundary of the SB is smooth and does not exhibit fractal-like behavior.

Figure 11 shows a fractal-like non-escaping set with a large excitation amplitude $\frac{|P|}{x} = 1.6\,(N = 2, M = 1 \text{ and } x_l = -\infty)$. The large amplitude excitation and strong non-linearity of the problem at the boundary result in fractal-like SB boundaries.

5 | CONCLUSIONS AND SCOPE FOR FURTHER RESEARCH

SBs of the escape problem of a particle from an asymmetrically truncated quadratic potential well under harmonic excitation can be investigated using a new method for the estimation of the global optima of the sum of two harmonic functions with arbitrary amplitudes, frequencies and phase shifts proposed in this paper.

The usefulness of the method is revealed when the ratio of the excitation frequency and natural frequency of the potential is a rational number $(\frac{N}{M})$. The size of the SB increases compared with the case when the excitation frequency is

disturbed by an infinitesimal amount. The SB area can increase significantly. For some frequency ratio, no SB in the perturbed system exists, whereas the system with the unperturbed frequency possesses an SB.

Thus, the SB can be divided into two parts, an essential part (a circular disk), where there is no change under small perturbations of the frequency ratio, and an illusory part, where the frequency ratio disappears under the slightest disturbance. However, the annihilation of the illusory part of the SB is a slow process. The smaller the perturbation of the frequency is, the longer it takes. Hence, investigation on the time limited escape and corresponding SBs is an important topic for the future research.

The analytic estimation of the size of the SB can be performed as well. The obtained formula provides a good understanding about the effects of the selection of N and M. The area of the SB rapidly converges to the area of the essential SB when N or M increases.

As long as the excitation frequency is smaller than the natural frequency of the well, the prediction with regard to the size of the non-escaping set of ICs is very accurate. However, in case of an excitation with frequency higher than the linear eigenfrequency of the well, new non-escaping islands appear in the IC plane, as the excitation amplitude exceeds the critical forcing value. For large forcing amplitudes, the emerging non-escaping set can exhibit fractal-like shapes, and strong non-linear dynamic behaviors can be observed during the motion of the particle.

Several questions might arise with regard to the introduced estimation approach and its implications on escape dynamics, for example, whether the estimation method might be extended to the sum of more than two harmonic terms, or to the sum of general periodic functions. If so, is there a way to investigate non-quadratic potentials using the proposed method?

This problem can be investigated by introducing a small non-linearity in the force field acting on the particle. There is an open question: How these non-linearities would affect the regions of the non-escaping set, especially if the linearized eigenfrequency of the bottom part of the potential well and the frequency of the excitation are rationally related?

We hope that we can attract readers' attention to the fascinating problems of escape dynamics, which demonstrate the complexity and wide variety of emerging problems in the simplest escape model, considering the truncated quadratic potential under harmonic excitation.

ACKNOWLEDGMENTS

This study was funded by the Deutsche Forschungsgemeinschaft (DFG, German Research Foundation) under Project No. 508244284.

Open access funding enabled and organized by Projekt DEAL.

CONFLICT OF INTEREST STATEMENT

The authors declare that they have no conflict of interest.

ORCID

Attila Genda https://orcid.org/0000-0001-8061-8473

REFERENCES

[1] Landau, L.D., Lifshitz, E.M.: Mechanics, 3rd edn., Butterworth, Oxford (1976)
[2] Thompson, J.M.T.: Chaotic phenomena triggering the escape from a potential well. Engineering Applications of Dynamics of Chaos, CISM Courses Lectures 139, 279–309 (1991)
[3] Virgin, L.N., Plaut, R.H., Cheng, C.-C.: Prediction of escape from a potential well under harmonic excitation. Int. J. Non-Linear Mechan. 27(3), 357–365 (1992)
[4] Virgin, L.N.: Approximate criterion for capsize based on deterministic dynamics. Dyn. Stability Syst. 4(1), 56–70 (1989)
[5] Sanjuan, M.A.F.: The effect of nonlinear damping on the universal escape oscillator. Int. J. Bifurc. Chaos 9, 735–744 (1999)
[6] Kramers, H.A.: Brownian motion in a field of force and the diffusion model of chemical reactions. Physica 7(4), 284–304 (1940)
[7] Fleming, G.R., Hänggi, P.: Activated Barrier Crossing. World Scientific (1993)
[8] Antonio Barone, G.P.: Physics and Applications of the Josephson Effect. John Wiley and Sons, Ltd (1982)
[9] Elata, D., Bamberger, H.: On the dynamic pull-in of electrostatic actuators with multiple degrees of freedom and multiple voltage sources. J. Microelectromech. Syst. 15, 131–140 (2006)
[10] Leus, V., Elata, D.: On the dynamic response of electrostatic mems switches. J. Microelectromech. Syst. 17, 236–243 (2008)
[11] Younis, M., Abdel-Rahman, E., Nayfeh, A.: A reduced-order model for electrically actuated microbeam-based mems. J. Microelectromech. Syst. 12, 672–680 (2003)
[12] Alsaleem, F., Younis, M., Ruzziconi, L.: An experimental and theoretical investigation of dynamic pull-in in mems resonators actuated electrostatically. J. Microelectromech. Syst. 19, 794–806 (2010)

[13] Ruzziconi, L., Younis, M.I., Lenci, S.: An electrically actuated imperfect microbeam: dynamical integrity for interpreting and predicting the device response. Meccanica 48(7), 1761–1775 (2013)
[14] Zhang, W.-M., Yan, H., Peng, Z.-K., Meng, G.: Electrostatic pull-in instability in mems/nems: a review. Sensors Actuators A: Physical 214, 187–218 (2014)
[15] Mann, B.p.: Energy criterion for potential well escapes in a bistable magnetic pendulum. J. Sound Vib. 323(3), 864–876 (2009)
[16] Arnold, V.I., Iacob, A., Kozlov, V.V., Neishtadt, A.I.: Mathematical Aspects of Classical and Celestial Mechanics. Encyclopaedia of Mathematical Sciences, Springer, Berlin, Heidelberg (2014)
[17] Quinn, D.D.: Transition to escape in a system of coupled oscillators. Int. J. Non-Linear Mechanics 32(6), 1193–1206 (1997)
[18] Belenky, V.: Stability and Safety of Ships–Risk of Capsizing. The Society of Naval Architects and Marine Engineers (2007)
[19] Talkner, P., Hänggi, P.: New Trends in Kramers' Reaction Rate Theory. Springer, Berlin (1995)
[20] Gendelman, O.V.: Escape of a harmonically forced particle from an infinite-range potential well: a transient resonance. Nonlinear Dyn. 93(1), 79–88 (2018)
[21] Genda, A., Fidlin, A., Gendelman, O.: On the escape of a resonantly excited couple of particles from a potential well. Nonlinear Dyn. 104(1), 91–102 (2021)
[22] Rega, G., Lenci, S.: Dynamical integrity and control of nonlinear mechanical oscillators. J. Vib. Control 14, 159–179 (2008)
[23] Orlando, D., Gonçalves, P., Lenci, S., Rega, G.: Influence of the mechanics of escape on the instability of von Mises truss and its control. Procedia Eng. 199, 778–783 (2017)
[24] Habib, G.: Dynamical integrity assessment of stable equilibria: a new rapid iterative procedure. Nonlinear Dyn. 106(3), 2073–2096 (2021)
[25] Karmi, G., Kravetc, P., Gendelman, O.: Analytic exploration of safe basins in a benchmark problem of forced escape. Nonlinear Dyn. 106, 1–17 (2021)
[26] Gendelman, O.V., Karmi, G.: Basic mechanisms of escape of a harmonically forced classical particle from a potential well. Nonlinear Dyn. 98(4), 2775–2792 (2019)
[27] Karmi, G.: Analytic exploration of safe basins in a benchmark problem of forced escape, (2022). https://www.graduate.technion.ac.il/Theses/Abstracts.asp?Id=33683.

How to cite this article: Genda, A., Fidlin, A., Gendelman, O.: Dynamics of forced escape from asymmetric truncated parabolic well. Z Angew Math Mech. e202200567 (2023). https://doi.org/10.1002/zamm.202200567